eprints@whiterose.ac.uk
https://eprints.whiterose.ac.uk/

Temperature Dependent Segregation in Alcohol-Water Binary Mixtures is Driven by Water Clustering

Samuel Lenton,[†,¶] Natasha H. Rhys,[†,§] James J. Towey,[†] Alan K. Soper,[*,‡,∥] and Lorna Dougan[†]

†*School of Physics and Astronomy, University of Leeds, LS2 9JT, UK*

‡*ISIS Facility, STFC Rutherford Appleton Laboratory, Harwell Campus, Didcot, OX11 0QX, UK*

¶*Current address: Department of Biology, University of York, York YO10 5DD, UK*

§*Current address: Department of Biochemistry, University of Oxford, Oxford, OX1 3QU, UK*

E-mail: soper866@btinternet.com

Abstract

Previous neutron scattering work, combined with computer simulated structure analysis, has established that binary mixtures of methanol and water partially segregate into water-rich and alcohol-rich components. It has furthermore been noted that, between methanol mole fractions of 0.27 and 0.54, both components, water and methanol, simultaneously form percolating clusters. This partial segregation is enhanced with decreasing temperature. The mole fraction of 0.27 also corresponds to the point of maximum excess entropy for ethanol-water mixtures. Here we study the degree of molecular segregation in aqueous ethanol solutions at a mole fraction of 0.27 and compare it with that in methanol-water solutions at the same concentration. Structural information is extracted for these solutions using neutron diffraction coupled with empirical potential structure refinement. We show that ethanol, like methanol, bi-percolates at this concentration and that, in a similar fashion to methanol, alcohol segregation, as measured by the proximity of neighboring methyl sidechains, is increased upon cooling the solution. Water clustering is found to be significantly enhanced in both alcohol solutions compared to the water clustering that occurs for random, hard sphere-like, mixing with no hydrogen bonds between molecules. Alcohol clustering via the hydrophobic groups is, on the other hand, only slightly sensitive to the water hydrogen-bond network. These results support the idea that it is the water clustering that drives the partial segregation of the two components, and hence the observed excess entropy of mixing.

Introduction

When two liquids mix, it is well known that the ideal entropy of the mixture, which is calculated by assuming the two liquids can completely inter-penetrate, has to be greater than the sum of entropies of the pure components on their own. This is because excess work would need to be done on the mixture once it is formed in order to render it unmixed. In practice molecular forces between the components can alter the actual mixed-state entropy either above or below the ideal value. In the case of a number of alcohol-water binary mixtures the

2

excess entropy of mixing is negative compared to the ideal mixing value.[1] Explanations for this negative excess entropy of mixing, which is seen in a number of aqueous mixtures, go back to at least 1945 when Frank and Evans suggested it indicated some sort of re-ordering in the solution, and proposed a model of water restructuring itself in an ice-like manner around the hydrophobic sidechains.[2]

How that ordering manifests in practice has been the subject of an extensive debate. Good examples of binary mixtures that display such properties are methanol and ethanol in water.[3–9] It is thought that the increase in ordering of these binary mixtures is the result of water and alcohol cluster formation.[4,10] According to that view cluster formation is driven by the amphiphilic nature of the alcohol, as a result of which the so-called "hydrophobic" regions cannot form hydrogen bonds, leaving the polar OH group free to hydrogen bond with water.[4] Compared to a typical chemical bond hydrogen bonds are relatively weak and can be made and broken by changes of temperature. It has been shown for methanol that a reduction of temperature is associated with an increase in the observed clustering in methanol-water binary mixtures, a direct result of increased hydrogen bonding between alcohol and water as the temperature is lowered.[4,6]

The importance of hydrogen bonds can be observed in more complex solutions such as those containing biological macromolecules or polymers. However, here we focus on simple alcohol systems, as a model to provide information about the effect of changing the non-polar chain on the hydrogen bond network in solution. The measured negative excess entropy of mixing is larger in ethanol-water solutions then for methanol-water,[1] caused, it is proposed, by the increased length of the hydrophobic region.[11] The measured excess entropy is also concentration dependent and for methanol it reaches a minimum around a mole fraction, $x = 0.36$, while for ethanol the minimum occurs near $x = 0.27$.[1] It is also at these concentrations of alcohol in water where many transport coefficients and thermodynamic functions have extremal values, thereby implying some kind of relationship between the previously observed clustering and thermodynamic properties at this concentration.[12,13] According to

3

the clustering theory for excess entropy of mixing of ethanol, increasing the sidechain length should result in increased cluster formation, driven by the extra non-polar methyl group present on ethanol.[14]

However, recent experimental work has suggested that the observed clustering in alcohol water binary mixtures is in fact a result of random interactions between sidechains, rather than driven by specifically hydrophobic effects.[15,16] Other studies have presented evidence that suggests otherwise, using computer simulation, neutron diffraction, X-ray absorption and emission studies.[17–20] Here we study the effects of the amphiphilic nature of alcohol on cluster formation at two temperatures. We use a combination of neutron diffraction with hydrogen isotope labeling and analysis by empirical potential structure refinement (EPSR)[21,22] to study segregation in solutions of ethanol and methanol in water at the same mole fraction for both alcohols ($x = 0.27$), and the effect of reducing the temperature on cluster formation. The neutron diffraction experiment provides unique information about the hydrogen bonding network by exploiting the difference in neutron scattering lengths between different isotopes of hydrogen, giving direct information about how hydrogen atoms are coordinated in solution. The data indicate that ethanol-water binary mixtures show a similar tendency to form clusters as methanol binary mixtures and that the effect increases as the temperature is lowered. In the present instances the clustering appears to be driven by the pronounced hydrogen bond association between water and the hydroxyl headgroups, rather than due to any special hydration effects around the hydrophobic regions of the alcohol molecules.

Methods

Neutron diffraction

Protiated and deuteriated samples of methanol, ethanol and water were obtained from Sigma Aldrich and used without further purification. Neutron diffraction measurements were performed on the NIMROD diffractometer at the ISIS pulsed neutron facility at the Rutherford

Appleton Laboratory in the UK. The data were corrected for beam attenuation, detector efficiency, inelastic and multiple scattering using the Gudrun software.[23] Furthermore the data were normalized against the scattering from a vanadium standard sample to obtain the final differential scattering cross section ($F(Q)$) on an absolute scale of differential scattering cross section per atom.

A well known problem with neutron scattering from materials containing hydrogen is the recoil of hydrogen (analogous to the electron recoil that causes Compton scattering with X-rays). With time of flight neutron diffraction this is exacerbated at low Q values.[24] There is no direct way to remove this effect so in this work we have used the iterative process proposed by Soper,[25] which involves making an initial estimate of the scattering angle averaged energy (or wavelength) dependent scattering, and use this as the underlying recoil scattering component to subtract from the estimated interference scattering, $F(Q)$. This process is repeated until convergence is achieved, although even this does not guarantee full removal of all inelasticity effects, since in practice the recoil scattering will itself be angle dependent to some extent.

For both alcohols, measurements were completed at an alcohol mole fraction of 0.27 at 298 K (25°C) and 245 K (-28°C). The lower temperature was chosen to be the lowest that could be reached without freezing in both solutions at this mole fraction.

The resulting $F(Q)$ is the sum of partial structure factors $H_{\alpha\beta}(Q)$ and can be written in terms of the atomic fraction, c, and corresponding scattering lengths, b, of atoms in the system:

$$F(Q) = \sum_{\alpha\beta} c_\alpha c_\beta \langle b_\alpha \rangle \langle b_\beta \rangle (2 - \delta_{\alpha\beta}) H_{\alpha\beta}(Q) \tag{1}$$

where Q is the change in momentum vector by the scattered neutrons, c_α and $\langle b_\alpha \rangle$ are the atomic fraction and neutron scattering length respectively for atom type α, the angle brackets on the latter indicating an average over the nuclear spin and isotope states of this

particular atom type. The partial structure factor, $H_{\alpha\beta}(Q)$, is the Fourier-transform of the corresponding site-site radial distribution function (RDF), $g_{\alpha\beta}(r)$:

$$H_{\alpha\beta}(Q) = 4\pi\rho \int_0^\infty r^2(g_{\alpha\beta}(r) - 1)\frac{\sin Qr}{Qr}dr \qquad (2)$$

with ρ the total atomic number density of the mixture. Integration of $g_{\alpha\beta}(r)$ between r_1 and r_2 yields the coordination number of atoms of type β around atoms of type α, in the distance range $r_1 \leq r \leq r_2$:

$$N_{\alpha\beta}(r_1, r_2) = 4\pi\rho c_\beta \int_{r_1}^{r_2} r^2(g_{\alpha\beta}(r))dr \qquad (3)$$

Atomic isotopes can have different neutron scattering lengths ($\langle b_\alpha \rangle$), for example the neutron scattering length of hydrogen is -3.74 fm, whereas that of deuterium is +6.67 fm. Therefore it is possible to modify the contributions of $H_{\alpha\beta}(Q)$ towards the measured $F(Q)$ by changing the isotopic constituents of the scattering molecule(s). Assuming that the isotopic substitution does not alter the structure of the liquid or molecules, then each isotopically labeled sample yields different structural information about the solute. N isotopically different samples yields N different data sets from which the $H_{\alpha\beta}(Q)$, and consequently $g_{\alpha\beta}(r)$, can be obtained. In practice it is rarely possible to have sufficient isotopically distinct samples to be able extract all the $H_{\alpha\beta}(Q)$ directly from the measured data. Therefore a computational method is required to estimate approximately the individual $g_{\alpha\beta}(r)$ functions present in the solution.

In the present experiment the label 'DD' refers to fully deuteriated alcohol mixed with heavy water, while 'HH' refers to fully protiated alcohol mixed with light water. Corresponding to these are the labels 'DH', which refers to fully deuteriated alcohol mixed with light water, and 'HD' which refers to protiated alcohol mixed with heavy water. For the latter two samples account must be taken of the exchange between hydroxyl hydrogen atoms and water hydrogen atoms when calculating the spin and isotope averaged scattering lengths for

these atoms.

Interpreting the data

To extract atom-scale information structural modeling is used with a set of constraints refined against the set of experimentally determined $F(Q)$. A simulation-assisted procedure, EPSR,[21,22] that has specifically been developed to convert the measured interference differential cross sections to real-space, is used here, thereby yielding estimated radial distribution functions of all atoms in the solution. This method, which is a variant of the reverse Monte Carlo method,[26] attempts to produce a structural model which provides the best overall agreement with the experimentally determined diffraction data. Although EPSR does not necessarily provide a unique structural interpretation of the experimental scattering data it does yield a model that is consistent with those data. EPSR has previously been used to study a wide range of biologically-relevant molecules in aqueous solution.[27–32]

In this paper we refer to the different atomic constituents of methanol and ethanol according to the chemical structures shown in Figure 1. Simulated boxes of molecules were constructed at the same concentration, temperature and atomic number density as the experimentally measured samples. Details of these boxes are given in Table 1.

Table 1: Details of the EPSR simulation boxes used in this work. In all cases the simulation boxes were cubic.

Alcohol	Methanol		Ethanol	
Temperature [°C]	+25°C	-28°C	+25°C	-28°C
Density [atoms/Å^3]	0.0982	0.1014	0.0994	0.1040
Simulation box dimension [Å]	33.854	33.494	35.957	35.412
No. of alcohol molecules in box	270	270	270	270
No. of water molecules in box	730	730	730	730

To start the simulation it is necessary to define an initial potential of interaction between the molecules. In the present case this consisted of a Lennard-Jones plus Coulomb interaction:
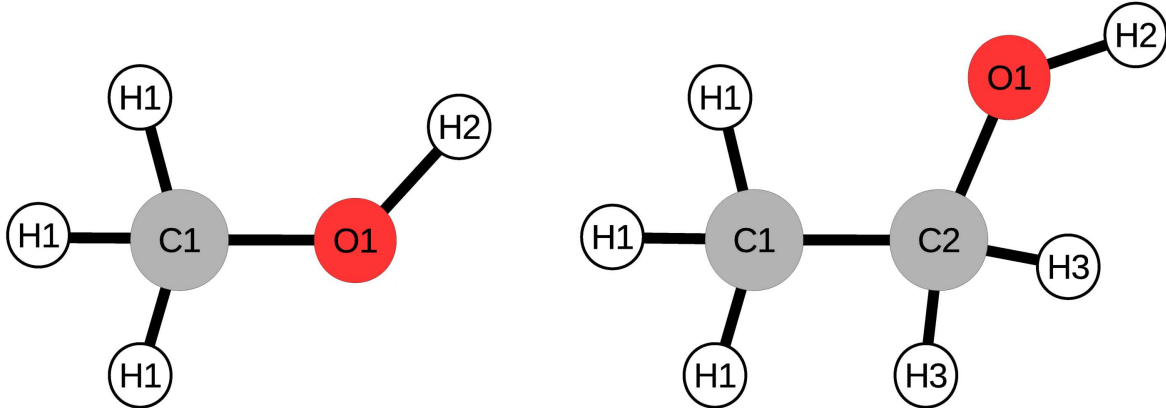
Figure 1: Atom labeling for the methanol (left) and ethanol (right) molecules used in EPSR analysis. All carbon atoms are labeled 'C1' or 'C2', the hydroxyl oxygen atom is labeled 'O1', with the corresponding hydroxyl hydrogen atom labeled 'H2'. The alkyl hydrogen atoms are labeled 'H1' or 'H3' depending on whether they are bonded to the C1 or C2 atoms respectively. Water oxygen and hydrogen atoms (not shown here) are labeled 'OW' and 'HW' respectively.

$$U_{\alpha\beta}(r) = 4\epsilon_{\alpha\beta} \left(\left(\frac{\sigma_{\alpha\beta}}{r} \right)^{12} - \left(\frac{\sigma_{\alpha\beta}}{r} \right)^{6} \right) + \frac{q_\alpha q_\beta}{4\pi\epsilon_0 r} \tag{4}$$

where $\epsilon_{\alpha\beta} = \sqrt{\epsilon_\alpha \epsilon_\beta}$, $\sigma_{\alpha\beta} = (\sigma_\alpha + \sigma_\beta)/2$, and q_α is the partial charge on atom α.

Table 2: Potential parameters for methanol (atoms labeled according to Fig. 1) used in the EPSR simulations of methanol-water solutions.

Atom Label	ϵ [kJ/mol]	σ [Å]	q [e]
C1	0.390	3.700	0.29700
O1	0.585	3.083	-0.72800
H1	0.065	0.000	0.00000
H2	0.000	0.000	0.43100

The likely parameters for this reference potential (RP) for the different atoms in these simulations can often be found from previous simulations, but the values used in the present work were mostly found by trial and error to give the best fits to the scattering data. The

Table 3: Potential parameters for ethanol (atoms labeled according to Fig. 1) used in the EPSR simulations of ethanol-water solutions.

Atom Label	ϵ [kJ/mol]	σ [Å]	q [e]
C1	0.800	3.700	-0.53825
C2	0.800	3.700	-0.04800
O1	0.650	3.100	-0.82375
H1	0.000	0.000	0.18365
H2	0.000	0.000	0.49175
H3	0.000	0.000	0.18365

Table 4: Potential parameters for water atoms used in the EPSR simulations of methanol-water and ethanol-water solutions.

Atom Label	ϵ [kJ/mol]	σ [Å]	q [e]
OW	0.650	3.166	0.84760
HW	0.000	0.000	-0.42380

values used are given in Tables 2-4. For methanol they are a modified version of the H1 potential given by Haughney et al,[33] the principle change being softened Lennard-Jones parameters for the methanol carbon atoms compared to the original potential. For ethanol, although other potential parameters are available,[34] these proved too soft when structure refinement was applied leading to unphysical overlaps between atoms. Instead the Lennard-Jones parameters were set to the default values used in the EPSR package, while the Coulomb charges were derived from a MOPAC7 refinement[35] of the structure of an isolated ethanol molecule, multiplied by a factor of 2.5 so that the charge on the oxygen atom was about the same as that on a water oxygen atom. The aim here was to ensure that any differences between ethanol and methanol that might be observed by the final analysis was driven by the data rather than by the underlying reference potential. However the uncertainty of these values highlights the uncertainties that still exist in the underlying potential parameters for alcohols and water. The potential parameters for the water molecules in both methanol and ethanol solutions were those of the SPC/E potential,[36] used without modification.

Truncation of the Coulomb potential is achieved using the reaction field method of Hummer et al.[37] Starting from a completely random distribution of molecules, the Monte Carlo

simulation is initially run with this interaction potential on its own to produce a configuration of molecules that satisfies realistic constraints on atomic overlap and likely hydrogen bonding interactions. In addition to the reference potential, the molecular conformation (bond lengths, bond angles, and dihedral angles) of each molecule is held in place by means of a series of harmonic pair interaction forces.[38] Use of these harmonic forces means the molecules have some degree of flexibility - controllable by the user - which mimics that observed in the real system.

Once the simulation with the reference potential has reached equilibrium, a perturbation of this potential, called the empirical potential (EP) is added to the reference potential to attempt to drive the simulation as close as possible to the measured data. The detailed method for deriving this perturbation is described elsewhere.[22] In achieving this, the presence of isotopically substituted samples, combined with use of a realistic reference potential, goes a long way to help identify the different contributions in equation (1): for methanol-water there are 21 contributions to (1), while for ethanol-water there are 36 such terms. The simulation is then run with this revised combined interaction potential (RP + EP). At regular intervals the EP is reassessed to see if the fit to the measured data can be improved. Once no further improvements are possible, a variety of distribution functions can be estimated from the simulation boxes and the ensemble average of these distribution functions calculated.

Results

Fits to the data

Figure 2 shows the total interference functions, $F(Q)$, obtained from the neutron diffraction experiments and corresponding fit obtained from the EPSR simulation. All isotopically distinct solutions of both alcohol solutions at both temperatures show a reasonable fit between EPSR simulation and the experimental data. There is a slight disagreement at low Q caused by difficult-to-remove inelastic scattering contributions from hydrogen in the sam-

ple. The main peak in the D-D solutions appears around 1.6-1.8 Å^{-1}, and is shifted to slightly lower values in ethanol (1.6 Å^{-1}) compared to methanol solutions (1.8 Å^{-1}) (Figure 3), which suggests the average intermolecular spacing in ethanol-water is slightly larger than in methanol-water, as might be expected from the relatively larger volume of the ethanol molecule compared to methanol. There are also some changes observed in the higher Q region that arise primarily from differences in the structure of the ethanol molecule compared to methanol and its impact on the local water structure.
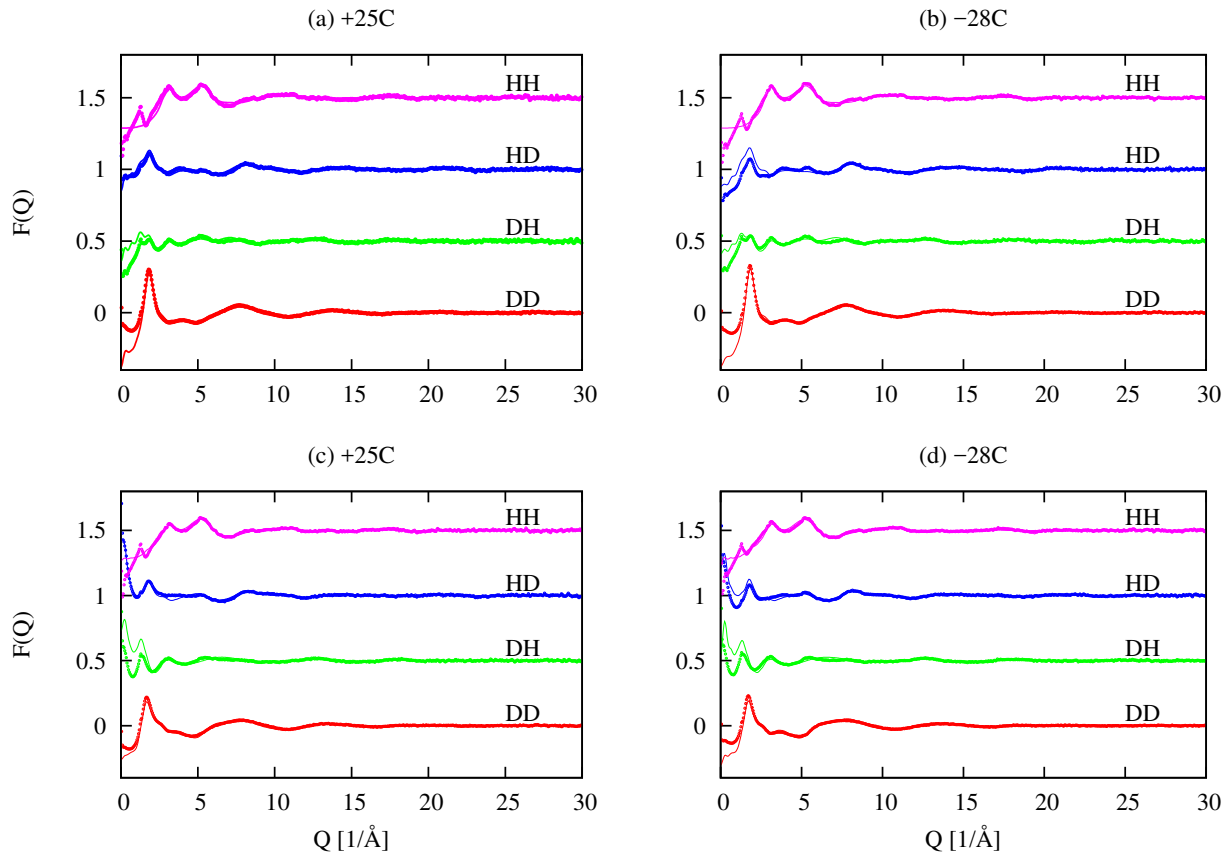

Figure 2: Fits of the EPSR simulation to the experimentally measured neutron differential cross section data for methanol ((a),(b)) and ethanol ((c),(d)) at +25°C ((a),(c)) and -28°C ((b),(d)) in an aqueous solution of molar ratio alcohol:water of 27:73. Curves are shifted vertically for clarity. Units of the differential cross sections are barns/atom/sr. (1 barn = 10^{-28} m^2)
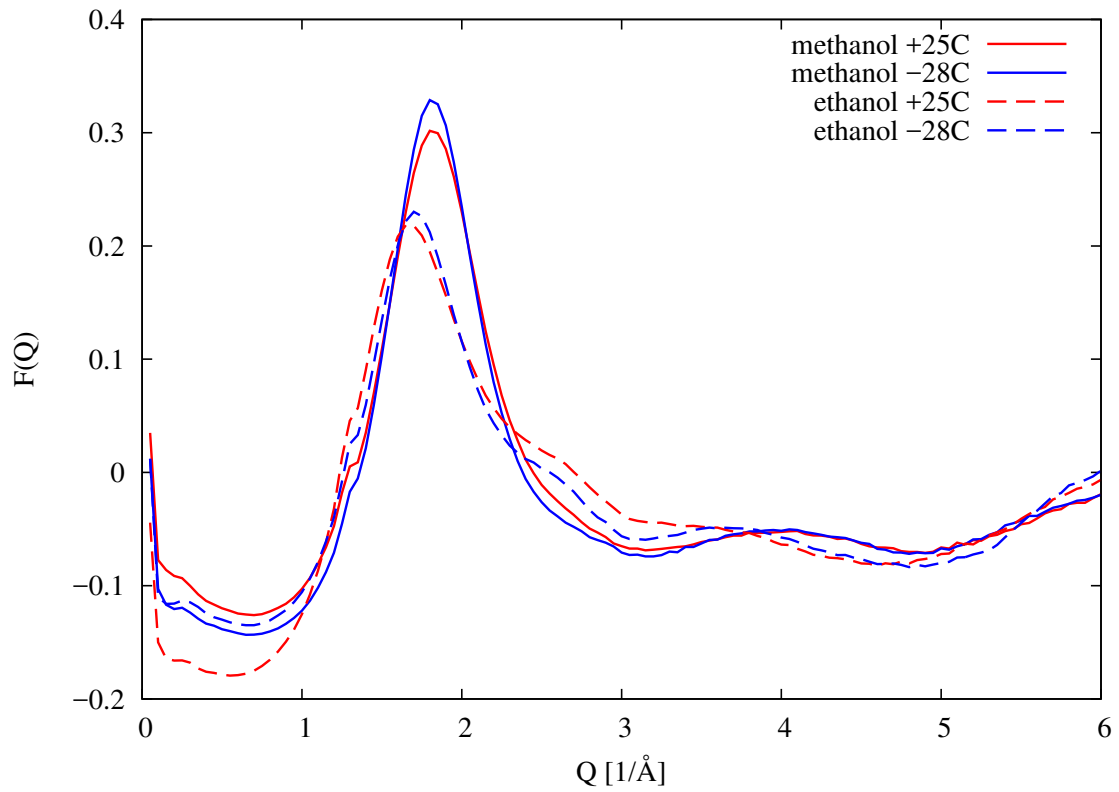
Figure 3: Zoom in on the neutron diffraction $F(Q)$ data of deuterated alcohols in deuterated water shown for ethanol and methanol at different temperatures. Units of the differential cross sections are barns/atom/sr. (1 barn = 10^{-28} m^2)

Water structure

From the EPSR simulation a variety of information can be extracted concerning the structure of the solutions. The oxygen-oxygen radial distribution functions (RDFs) obtained from the EPSR simulations for water oxygens in both alcohol solutions at both the measured temperatures are shown in Fig. 4 alongside the same RDF obtained for pure water.[25] Two distinct peaks are observable for both solutions, the first peak at 2.7-2.8 Å corresponds to the first water hydration shell, whilst the second major peak at around 4.5 Å is traditionally assigned to the tetrahedral structure of water in solution. As the temperature is lowered the peak intensities rise somewhat, signaling an increase in the water tetrahedral structure.
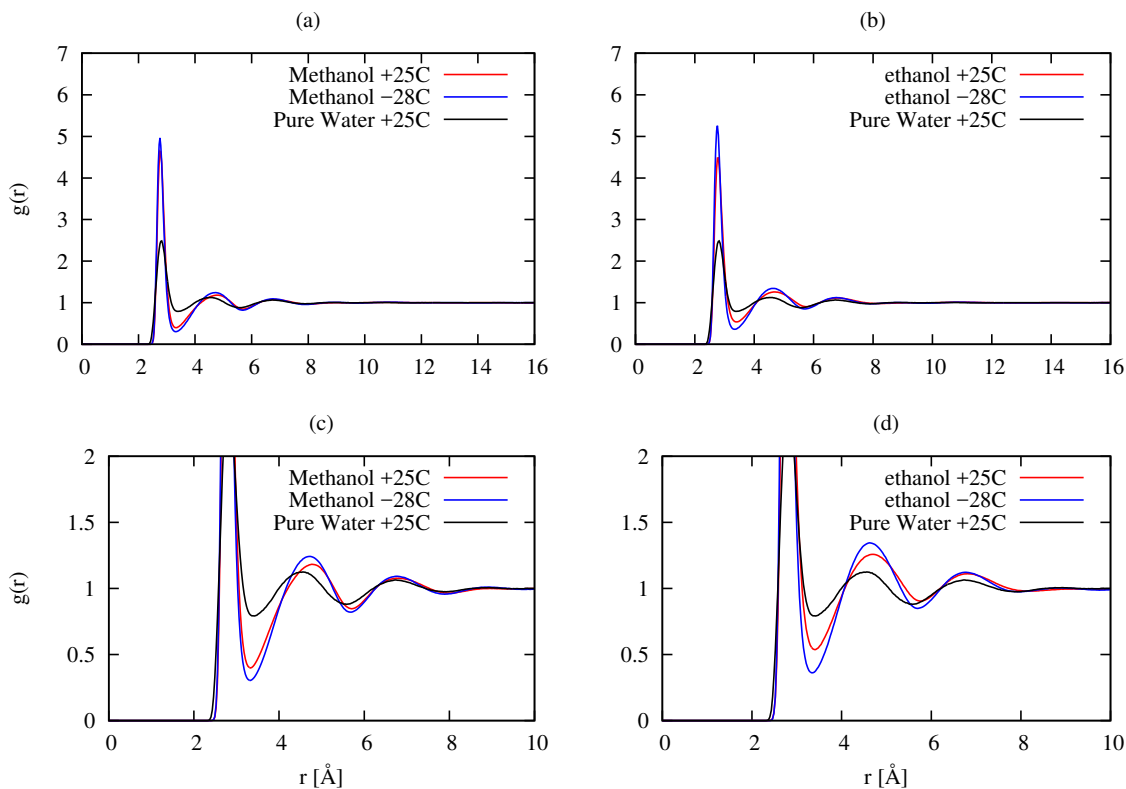

Figure 4: Site-site radial distribution functions between water oxygen shown for (a), the methanol water solutions and (b) the ethanol water solutions. Bottom: (c) and (d), enlarged section of the RDFs shown above, highlighting the tetrahedral water interaction for both alcohol solutions.

For both the methanol-water and ethanol-water solution there is a marked difference in

the heights of these peaks compared to bulk water. Whilst it is tempting to assign this difference to water structuring effects caused by the alcohol, it must also be borne in mind that because most water molecules will be in the vicinity of an alcohol molecule, excluded volume effects can be a major additional factor in making the water appear more structured than it actually is.[39] From that analysis the size of the excluded volume effect on the water structure at low r relates directly to the inverse of the water volume fraction in solution, while the range in r of the effect relates to the size of the cavities created by the solute. Based on the known densities of the pure components, it is possible to estimate approximately the water volume fraction in each solution. For a mole fraction of 0.27 alcohol in water, the estimated water volume fractions are 0.55 for methanol:water, and 0.46 for ethanol:water. This means the amplification factor from excluded volume effects of the small r features in Fig. 4 will be of order 1.8 for methanol in water and 2.2 for ethanol in water. Visual inspection of Fig. 4 suggests that the observed differences between water in solution and pure water are in line with these factors at the lower r values, and hence cannot be taken as clear evidence for enhanced water structure in these alcohol-water solutions compared to bulk water. Such a sharpening of the first peaks in methanol-water solutions was also observed in our earlier data[4,6] but is better resolved here due to the improved counting statistics at intermediate Q values, which arise from using the NIMROD diffractometer at ISIS compared to the previous SANDALS diffractometer, and also the revised method of removing inelasticity effects employed in this work.[25]

The results for ethanol appear similar to those for methanol, although the main peaks are even sharper, a consequence no doubt of the larger size of the ethanol molecule compared to methanol creating a larger excluded volume effect, as described above. To further study the effects of the two different alcohols on the water structure the triplet bond angle distribution of water was obtained (Ow-Ow-Ow, Fig. 5). In this case two water molecules are regarded as "bonded" if their oxygen atoms are separated by 3.3Å or less. This distribution was calculated for each of the alcohol-water solutions shown here, as well as for pure water,

14

using the neutron and x-ray data presented in.[25] The triplet bond angle distribution shows a broad peak around 110°, corresponding to the tetrahedral structure of water in both alcohol solutions, and which appears similar in ethanol-water compared to methanol-water, but markedly enhanced compared to pure water. There is also a small peak near 57° which arises from triplets of water molecules at their nearest neighbour distances. Such water molecules involve included angles of $\sim 60°$ and so cannot be hydrogen bonded. They are commonly observed in distributions of this kind. See for example Fig. 3 of.[40] Again there is a temperature dependence observed resulting in an increase of water tetrahedrality as the temperature is lowered.

These trends can be quantified by calculating the tetrahedral order parameter, q:

$$q = 1 - \frac{9}{4}\left[\int_0^\pi P(\theta)\sin\theta\left[\cos\theta + \frac{1}{3}\right]^2 d\theta\right] \bigg/ \left[\int_0^\pi P(\theta)\sin\theta\, d\theta\right] \tag{5}$$

where $P(\theta)$ is one of the bond angle distributions shown in Fig. 5, and the normalisation is chosen so that $q = 1$ for a perfectly tetrahedral system, and $q = 0$ for a uniform distribution of bond angles.[41] The calculated values of this parameter are given in Table 5.

As can be seen from this table, the values of q for methanol and ethanol in solution are markedly higher than for pure water at the same temperature, and these values increase as the temperature is lowered. The methanol values are slightly larger than for ethanol, mirroring the small differences in the bond angle distributions between methanol and ethanol seen in Fig. 5.

Table 5: Tetrahedral order parameter q, equation (5), for alcohol-water solutions.

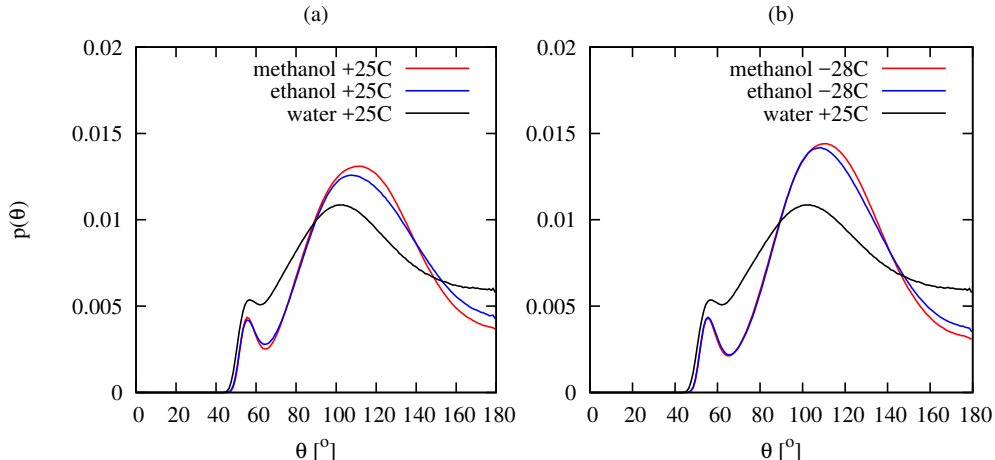| Sample	q
Pure water 25°C	0.564
Methanol-water 25°C	0.668
Ethanol-water 25°C	0.655
Methanol-water -28°C	0.693
Ethanol-water -28°C	0.685

15

Figure 5: Triplet bond angle distribution (Ow-Ow-Ow) shown for the alcohol solutions at 25°C (a) and -28°C (b). Two water molecules are regarded as "bonded" if their oxygen atoms are separated by 3.3 Å or less. Also shown is the triplet bond angle distribution for pure water, calculated with the same criterion as for the alcohol solutions.

Another feature of Fig. 5 and Table 5 is that water in methanol-water appears slightly more tetrahedral than in ethanol-water. To understand this, it necessary to realise that because the alcohol solutions are at the same mole fraction, this means the volume fraction occupied by ethanol will be larger than the volume fraction occupied by methanol - simply because of the larger size of the ethanol molecule. Conversely the volume fraction occupied by the water will be less in ethanol-water than in methanol-water, which might induce this small difference in the degree of tetrahedrality.

In order to further show the differences in water structure between pure water and alcohol-water, in Fig. 6 we compare the spatial density function (SDF) for water around water in ethanol-water at 25°C with the same distribution in pure water at the same temperature. The SDF, originally invented by Shishchev and Kusalik[42] shows the 3-dimensional pair distribution function of molecules around a central molecule, and is plotted as a surface contour which encloses a certain fraction of the all the molecules within a specified distance range. In the present case the distance range is 0 - 5 Å from the central molecule, and the contour level is set to capture 60% of all the molecules in this range, for both ethanol-water and pure water.

In both cases an inner coordination sphere with near tetrahedral geometry can be seen, and an outer coordination sphere which is in almost exact anti-phase with the inner coordination sphere. In the case of pure water this outer coordination sphere joins on to the inner coordination sphere in places, while in ethanol-water, the two coordination spheres are completely separate. A similar effect has been seen comparing high density and low density amorphous ices,[43], and shows the strong expansion effect (lowering the density) ethanol has on water structure.
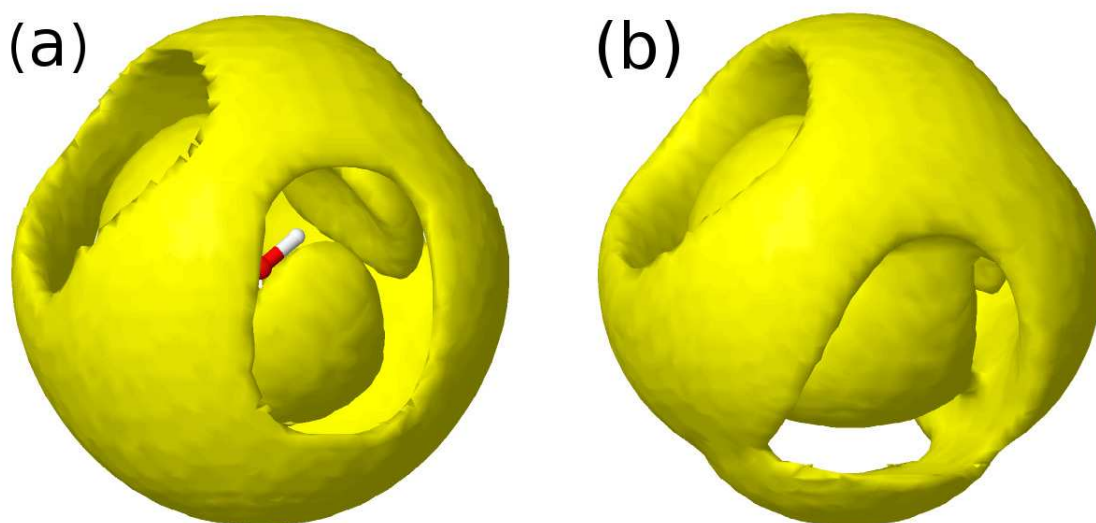

Figure 6: Spatial density function for water around water in ethanol-water, mole fraction 0.27, (a) and in pure water at the same temperature (25°C) (b). The contour level is chosen in each case to capture 60% of the molecules in the distance range 0 - 5 Å. In both cases the outer diameter of the plot is 10 Å.

Alcohol-alcohol interactions

Figure 7 shows the radial distribution functions determined from the EPSR simulation for alcohol-alcohol interactions in both binary mixtures. A comparison can be made between the methyl carbon atom (C1) on ethanol with the only carbon atom in methanol (also C1). In the ethanol-water binary mixture the methyl carbon atom (C1) is most likely to cluster with other ethanol molecules due to its lack of hydrophilicity relative to the hydroxyl

carbon atom (C2). The C1-C1 RDF obtained for methanol is in good agreement with previously published data, showing a first peak around $3.9\,\mathrm{\AA}$ and a second peak at $\sim7\,\mathrm{\AA}$. Upon decreasing the temperature the interaction between methanol molecules changes only marginally. For ethanol-ethanol interactions between the C1 carbons, the first peak in the RDF corresponds to the same distance $(4.0\,\mathrm{\AA})$ observed in methanol, however the peak now has a double peak structure, corresponding to the more complex packing of the hydrophobic chain of ethanol. Upon cooling, the interaction between ethanol molecules also changes to a greater extent to that observed in methanol.
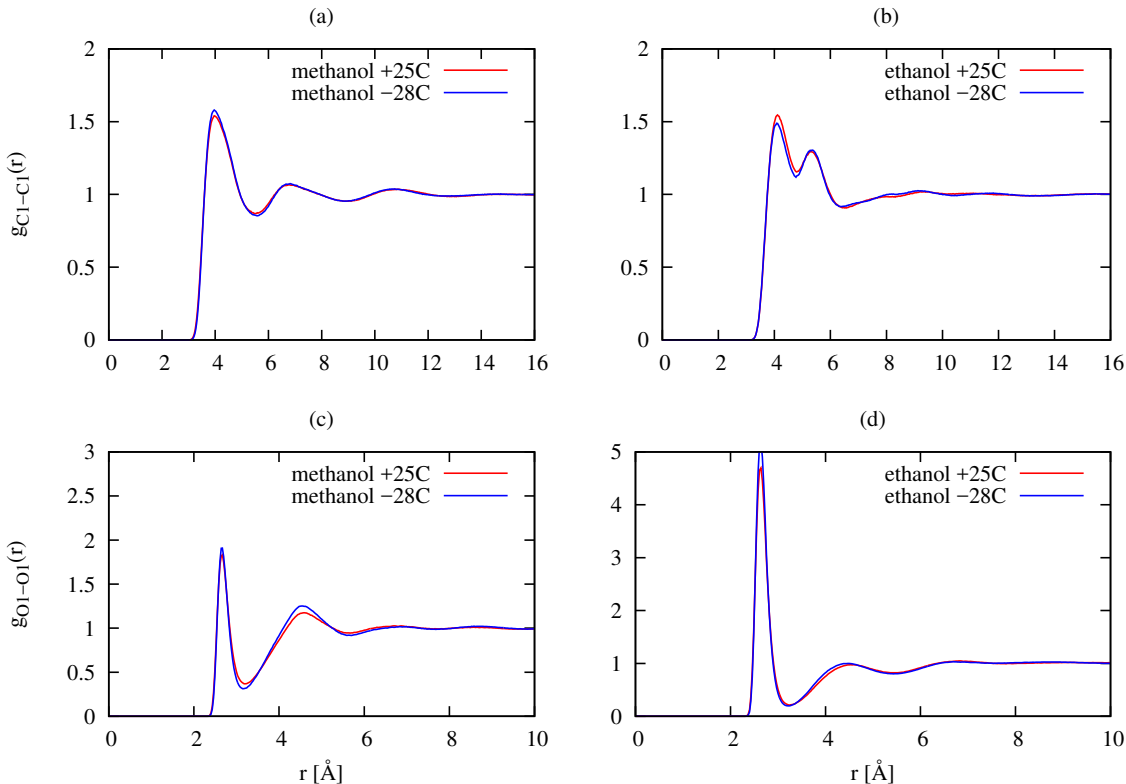

Figure 7: Site-site radial distribution functions showing the interactions between alcohol molecules at the different temperatures measured. Top: The hydrophobic methyl carbons and Bottom: The hydrophilic hydroxyl oxygens.

Comparing these hydrophobic interactions with the hydrophilic, O1-O1 interaction, there is a marked difference between the two alcohols. For methanol, the coordination number of the first peak, integrated out to $3.2\,\mathrm{\AA}$ is 0.45 ± 0.05 while for ethanol the coordination number

for the same peak, and to the same distance is 0.70 ± 0.05, so signifying an enhanced hydrogen bond interaction between ethanol molecules in solution compared to methanol. The effect of temperature on this interaction is however marginal.

Alcohol-water interactions

Fig. 8 shows the hydration of the same oxygen and carbon atoms at the different temperatures. For the hydrophilic site the O1 oxygen atom coordinates about 2.1 ± 0.1 water molecules for both alcohols, where, like pure water, this number includes some non hydrogen-bonded water molecules. The RDFs of water around the carbon atoms is more complex due to the geometry of the methanol and ethanol molecules, although it will be noted that the C1-OW interaction in methanol-water is more similar to the C2-OW interaction in ethanol than it is to the C1-OW interaction in ethanol. This emphasizes the pronounced hydration of both alcohols around their respective hydroxyl groups.
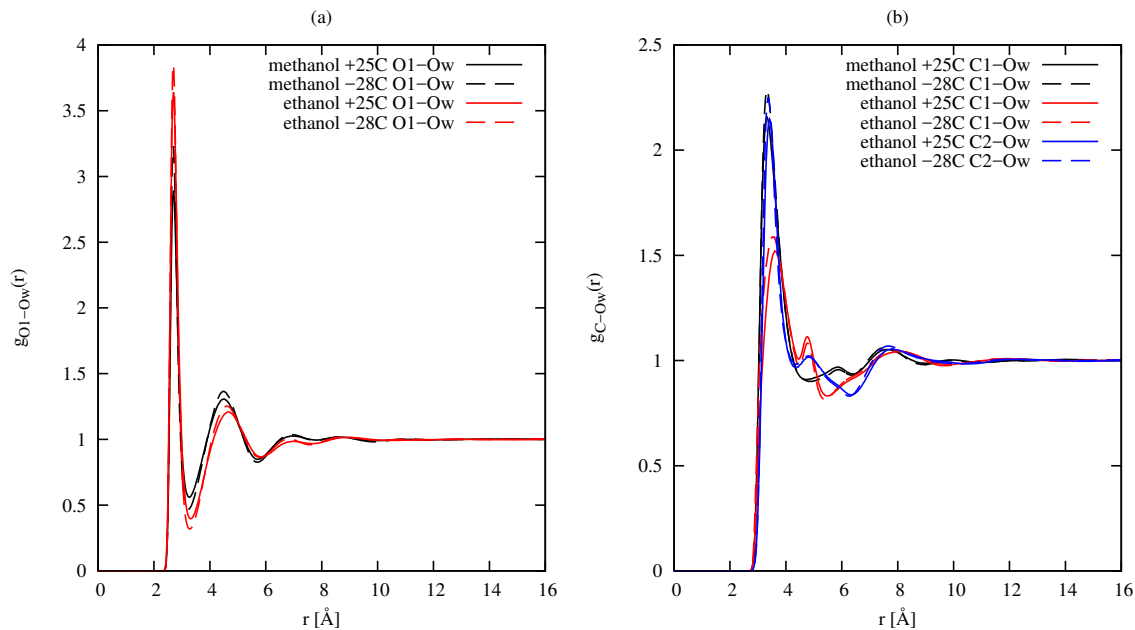

Figure 8: Hydration radial distribution functions of alcohol oxygen (O1) (a) and carbon (C1,C2) (b) atoms at different temperatures. For ethanol C1 represents the carbon on the methyl group and C2 the carbon on the hydroxyl group.

19

Cluster analysis

To obtain further information on the degree of molecular segregation in these solutions we now proceed to use cluster size analysis on the water and alcohol molecules in solution, based on the current EPSR simulations. Clustering of both species in each binary mixture was determined by using the cluster analysis routine within EPSR. For clusters involving only water molecules, two water molecules were considered to belong to the same cluster if their Ow-Ow distance was less than 3.3 Å, while for alcohol clusters, the criterion was for their respective C1 (or C2 in the case of ethanol) atoms, that is the hydrophobic sidechains, to be 5.0 Å or less apart. These distances are determined from the position of the first minimum after the main peak in the corresponding RDF. For the C1-C1 interaction this minimum distance is smaller than the 5.7 Å that was used previously [4] because of the more complex nature of the first peak in the C1-C1 interaction in ethanol compared to the same interaction in methanol - compare Figs. 7(a) with 7(b). Fig. 9 shows the cluster size distributions of water and alcohol clusters in the binary mixtures alongside the predicted percolation threshold power law $N(s) \sim s^{-2.2}$, which describes random percolation on a 3D lattice, where s is cluster size and $N(s)$ is the probability of finding a cluster of size s. We can say this because the probability for the largest clusters is well above the percolation threshold, meaning many if not most of these larger clusters will be percolating. Previously it has been observed that at the concentrations used in this study ($x = 0.27$) both water and methanol clusters percolate[4] and the present analysis agrees well with those earlier results. We here extend the observation of bipercolation to ethanol-water solutions at the same concentration (Fig. 9 (b) and (d)).

Because the majority of water or alcohols are in large percolating clusters, the effect of temperature on these cluster distributions is relatively weak. Nonetheless, it is generally true to say that as the temperature is lowered the fraction of alcohol molecules in smaller clusters (less than 100 molecules) decreases while the fraction in larger clusters increases. To make this point more quantitatively, the fractions of water and alcohol molecules in large
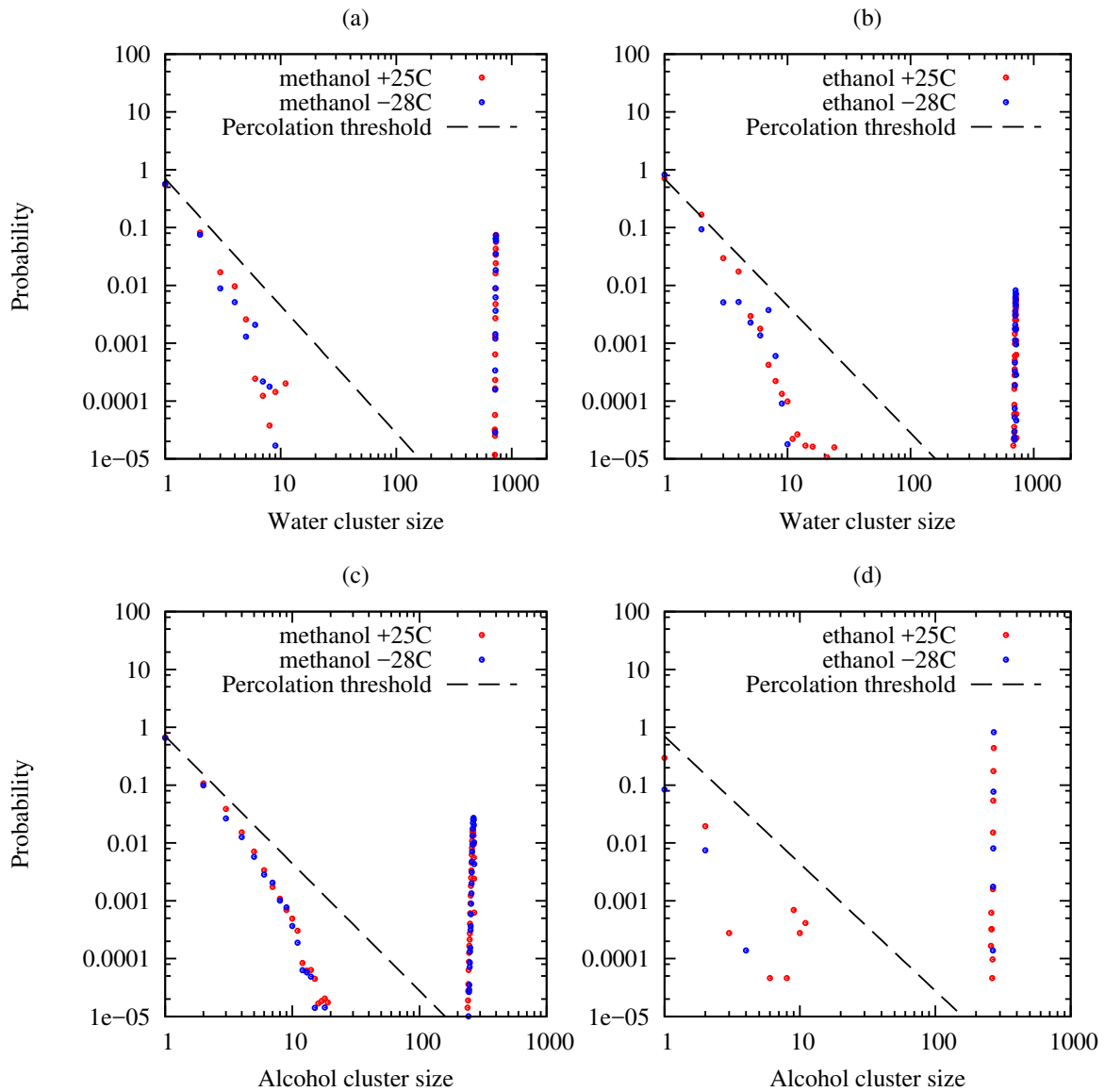
Figure 9: Cluster size distribution in alcohol-water solutions. (a) and (b) are for water clusters; (c) and (d) are for alcohol clusters. The distributions are shown for methanol ((a) and (c)) and ethanol ((b) and (d)). The dashed line shows the predicted distribution at the percolation threshold.

21

(greater than 100 molecules) clusters are shown in Figs. 10 (a) and (b) respectively, where, in addition, it can be seen that lowering the temperature generally tends to enhance the degree of clustering, although the effect is small due to the fact that most alcohol molecules are already in large clusters. We note that the fraction of water molecules in large clusters is slightly lower in ethanol solutions compared to methanol because water will have a smaller volume fraction in ethanol solution than in a methanol solution at the same molar ratio. The opposite is seen for the alcohol clusters, that is, large ethanol clusters are more likely to form than large methanol clusters. By the same token, according to Fig. 10, nearly 100% of ethanol molecules are in large clusters, while 97% of methanol molecules are in large clusters, so the distribution of small clusters in ethanol is relatively weak and noisy compared to the same distribution in methanol-water. Compare Fig. 9(d) with Fig. 9(c).

Discussion

As shown by Towey et al.,[44] when discussing clustering in these aqueous solutions it is important to establish the extent to which the observed clustering would have been observed in a randomly mixed solution. Because of the repulsive forces which prevent atomic overlap, the thermodynamically ideal "randomly mixed" state, where the solution components can occupy all of space uniformly, is not realizable. Instead, it is more informative to compare the observed structure and molecular clustering with what would be observed if all the hydrogen bonding between water molecules, between alcohol molecules, and between water and alcohol were switched off. To simulate this case, a parallel set of simulations of the alcohol-water mixtures were performed at the same mole fraction and with the same molecular geometries and Lennard-Jones parameters (Tables 2 - 4), but with all Coulomb charges and the empirical potential set to zero. These simulations were analyzed for clustering using the same criteria for bonding as used for the previous simulations. Fig. 10 compares the cluster distributions with and without hydrogen bonding at 25°C.

(a) Fraction of water in large clusters
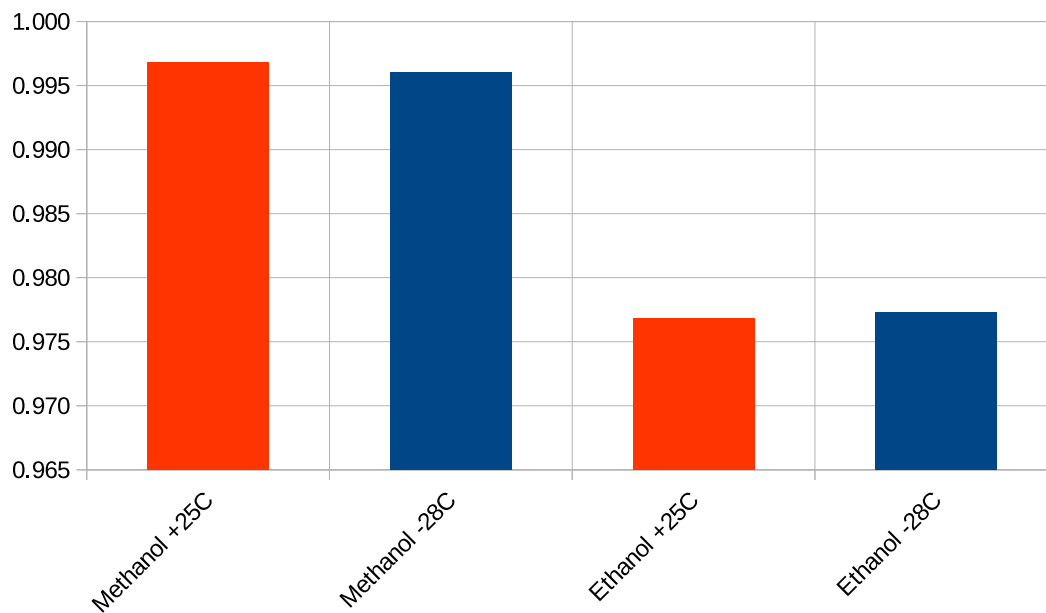
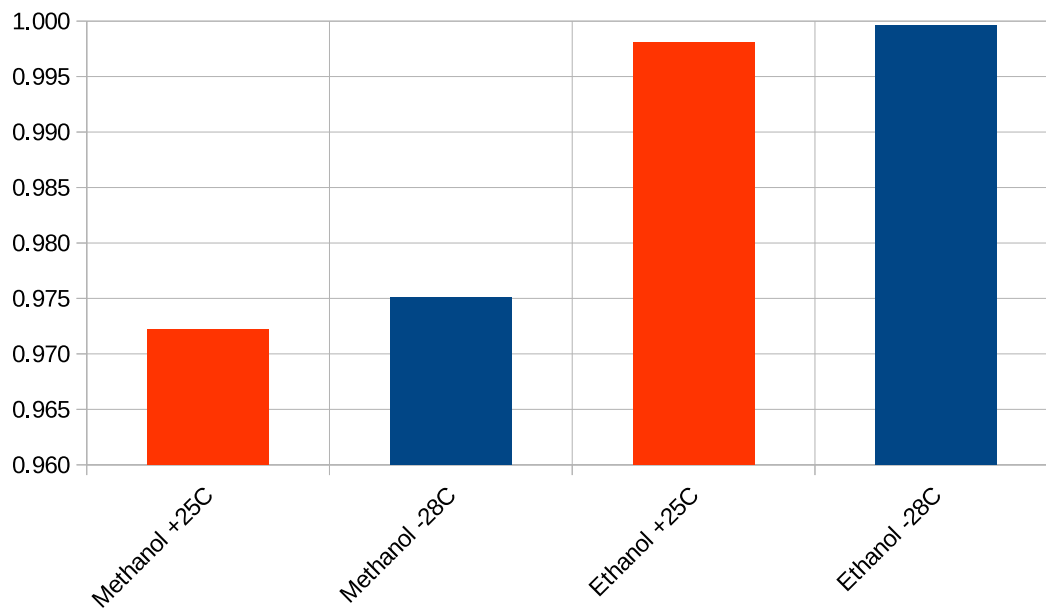## (b) Fraction of alcohol in large clusters

Figure 10: Fractions of water, (a), and alcohol, (b), molecules in large (> 100 molecules) clusters at two temperatures.
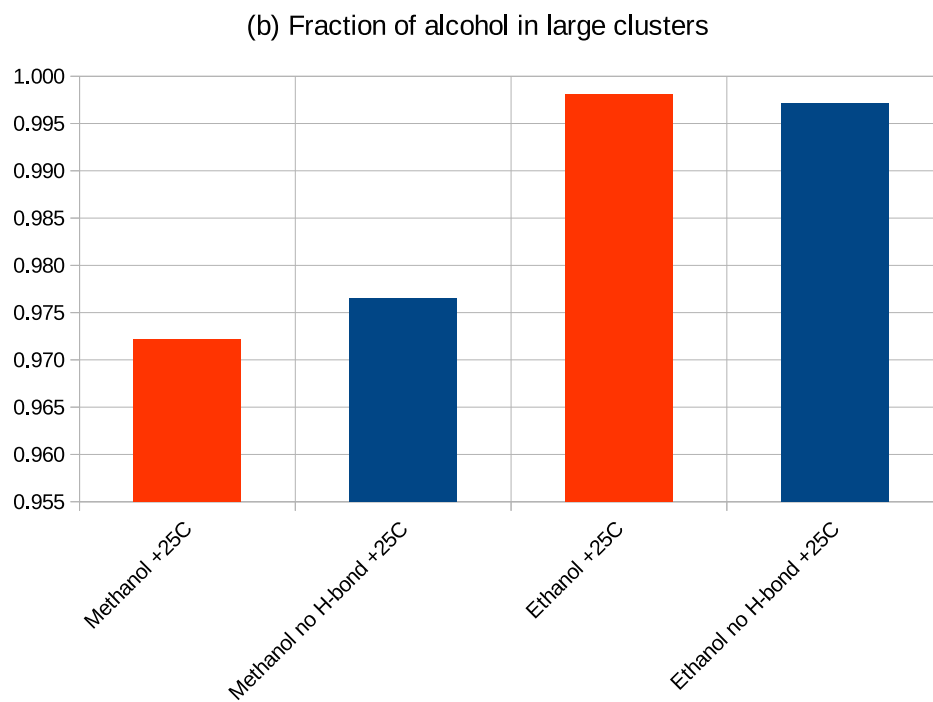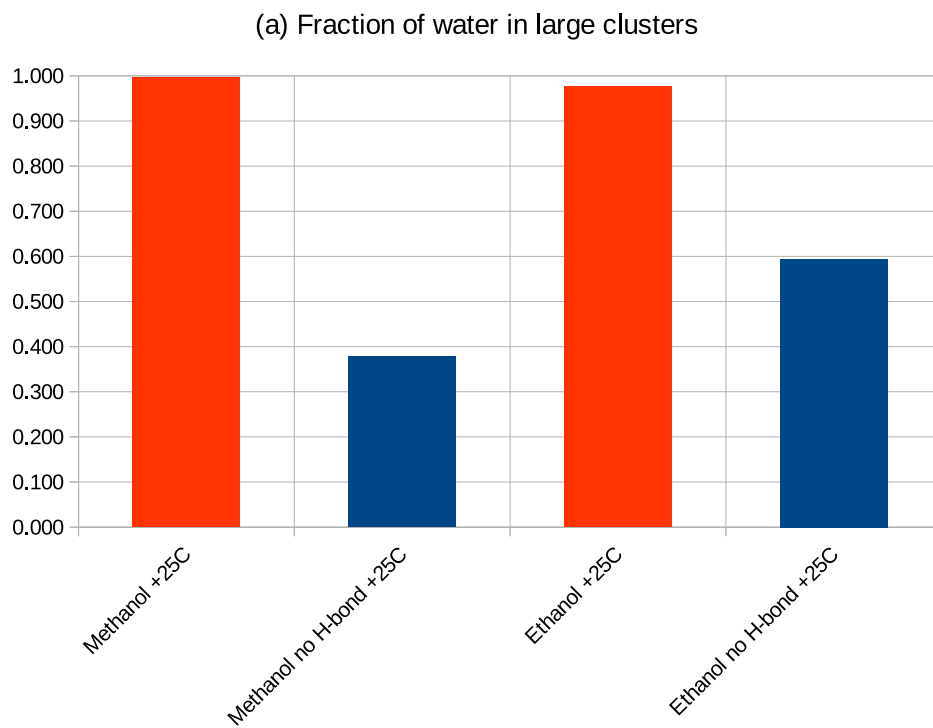
Figure 11: Fractions of water, (a), and alcohol,(b), molecules in large (> 100 molecules) clusters at 25°C with (orange) and without (blue) hydrogen bonding.

It can be seen that for the water clusters, switching on hydrogen bonding has a large impact on the fraction of water molecules in large clusters. When hydrogen bonding is not present (blue bars) the fraction of water in large clusters is between 40% (methanol) and 60% (ethanol) suggesting these clusters are barely percolating at this mole fraction, while when it is present (orange bars), most of the water is occurring in large clusters. On the other hand, for the alcohol clusters, which are defined via the contact distance between the methyl carbon atoms, C1 and C2, hydrogen bonding has only a marginal impact on the degree of clustering.

One conclusion from Fig. 11 therefore is that clustering of so-called hydrophobic entities is not necessarily driven by the presence or absence of a hydrogen bonding medium which surrounds them. According to the present analysis it can be regarded simply as a result of the natural overlap and dispersion forces that exist between all molecular entities. A similar conclusion could be drawn comparing the change in water correlation functions with temperature, Fig. 4 with the change in alcohol correlations with temperature, Fig. 7. Notable changes in the water correlation functions occur with temperature, while the corresponding alcohol correlation functions remain almost unperturbed. It is worth noting here that, Takamuku *et al.*[5], using X-ray diffraction on mixtures of methanol, ethanol and 2-propanol in water, independently concluded that it was mostly the water structure that changed noticeably over a similar temperature range. Equally the alcohol water correlations also change slightly with temperature, Fig. 8, which, together with Fig. 7, also suggests that it is the water structure that is temperature sensitive, and not the arrangement of alcohol molecules. Nonetheless, it is apparent from Fig. 10 that the degree of alcohol clustering increases slightly as the temperature decreases, particularly in the case of ethanol.

A recent paper by Davis et al.[45] concludes that the hydrophobic tails of monohydric alcohols induce a more structured form of water around them. They make this proposition based on the red-shift seen around the OH stretch frequency in Raman scattering data. Using solute-correlated spectra, they surmise that around such entities, the weaker hydrogen bonds

found in bulk water become depleted relative to the stronger tetrahedral bonds. However no explanation is given other than by reference to computer simulation analyses which show a similar behavior. A further useful review of this effect is given by Titantah and Karttunen.[46] The chosen mole fraction of that work, namely $x = 0.01$ is much lower than the $x = 0.27$ of the present work, making direct comparison unreliable. In the present case we *do* see enhanced tetrahedrality in the water structure of these concentrated alcohol solutions compared to pure water, Fig. 5 and Table 5, but this appears in our case to be related to the pronounced hydrogen bonding of water to the hydroxyl oxygen, Fig. 8(a), rather than a consequence of hydrophobicity.

Conclusion

In this work we have studied the hydrogen bond network present in ethanol-water binary mixtures and compared these to new data collected on the well-characterized methanol-water binary mixture at a single mole fraction ($x = 0.27$). The methanol-water data are in broad agreement to previously published work, but have better resolution. The new data show percolating cluster formation for both water and alcohol clusters, and for the alcohol clusters in particular the maximum cluster size tends to increase as the temperature is lowered.

In our new data ethanol-water binary mixtures apparently show a increased tendency for alcohol clustering when compared to methanol-water binary mixture at the same mole fraction. We argue that this is apparent primarily because the alcohol volume fraction in ethanol-water is higher than in methanol-water. Comparison with cluster formation in a simulation where all hydrogen bonding interactions are switched off suggests that hydrogen bonding is not primarily responsible for the alcohol clustering via the hydrophobic groups. Instead it appears to arise mainly from the overlap and dispersion interactions which occur between all molecular species in close proximity. In contrast, the hydrogen bond has a very pronounced effect on the degree of water clustering. Given the proposal by Chandler[47] that

true hydrophobic effects occur on length scales of 1 nm or more, it would appear that the present neutron scattering data from alcohol-water solutions support that view. At the same time the enhanced tetrahedrality of the water seen in this and other experiments appears to arise from the H-bonding of water to the alcohol hydroxyl group, rather than to any specific hydrophobic effect as others have speculated.

Acknowledgement

References

(1) Lama, R. F.; Lu, B. C.-Y. Excess Thermodynamic Properties of Aqueous Alcohol Solutions. *J. Chem. Eng. Data* **1965**, *10*, 216–219.

(2) Frank, H. S.; Evans, M. W. Free Volume and Entropy in Condensed Systems III. Entropy in Binary Liquid Mixtures; Partial Molal Entropy in Dilute Solutions; Structure and Thermodynamics in Aqueous Electrolytes. *J. Chem. Phys.* **1945**, *13*, 507.

(3) Matsumoto, M.; Nishi, N.; Furusawa, T.; Saita, M.; Takamuku, T.; Yamagami, M.; Yamaguchi, T. Structure of Clusters in Ethanol–Water Binary Solutions Studied by Mass Spectrometry and X-ray Diffraction. *Bull. Chem. Soc. Jpn.* **1995**, *68*, 1775–1783.

(4) Dougan, L.; Bates, S. P.; Hargreaves, R.; Fox, J. P.; Crain, J.; Finney, J. L.; Réat, V.; Soper, A. K. Methanol–Water Solutions: A Bi-percolating Liquid Mixture. *J. Chem. Phys.* **2004**, *121*, 6456–6462.

(5) Takamuku, T.; Saisho, K.; Nozawa, S.; Yamaguchi, T. X-ray Diffraction Studies on Methanol–Water, Ethanol–Water, and 2-Propanol–Water Mixtures at Low Temperatures. *J. Mol. Liq.* **2005**, *119*, 133–146.

(6) Dougan, L.; Hargreaves, R.; Bates, S. P.; Finney, J. L.; Réat, V.; Soper, A. K.; Crain, J. Segregation in Aqueous Methanol Enhanced by Cooling and Compression. *J. Chem. Phys.* **2005**, *122*.

(7) Allison, S. K.; Fox, J. P.; Hargreaves, R.; Bates, S. P. Clustering and Microimmiscibility in Alcohol–Water Mixtures: Evidence from Molecular-Dynamics Simulations. *Phys. Rev. B* **2005**, *71*, 024201.

(8) Yamaguchi, T.; Takamuku, T.; Soper, A. K. Neutron Diffraction Study on Microinhomogeneities in Ethanol–Water Mixtures. *J. Neutron Res.* **2005**, *13*, 129–133.

(9) Hsieh, W.-P.; Chien, Y.-H.; Shaner, J. W.; Steinberg, D. J.; Baonza, V. G. High Pressure Raman Spectroscopy of H2O-CH3OH Mixtures. *Sci. Rep.* **2015**, *5*, 8532.

(10) Dixit, S.; Crain, J.; Poon, W. C. K.; Finney, J. L.; Soper, A. K. Molecular Segregation Observed in a Concentrated AlcoholâĂŞWater Solution. *Nature* **2002**, *416*, 829–832.

(11) Lam, R. K.; Smith, J. W.; Saykally, R. J. Communication: Hydrogen Bonding Interactions in Water–Alcohol Mixtures from X-ray Absorption Spectroscopy. *J. Chem. Phys.* **2016**, *144*, 191103.

(12) Soliman, K.; Marschall, E. Viscosity of selected binary, ternary, and quaternary liquid mixtures. *J. Chem. Eng. Data* **1990**, *35*, 375–381.

(13) Derlacki, Z. J.; Easteal, A. J.; Edge, A. V. J.; Woolf, L. A.; Roksandic, Z. Diffusion Coefficients of Methanol and Water and the Mutual Diffusion Coefficient in Methanol–Water Solutions at 278 and 298 K. *J. Phys. Chem.* **1985**, *89*, 5318–5322.

(14) Soper, A. K.; Dougan, L.; Crain, J.; Finney, J. L. Excess Entropy in Alcohol-Water Solutions: A Simple Clustering Explanation. *J. Phys. Chem. B* **2006**, *110*, 3472–3476.

(15) Perera, P. N.; Fega, K. R.; Lawrence, C.; Sundstrom, E. J.; Tomlinson-Phillips, J.; Ben-Amotz, D. Observation of Water Dangling OH Bonds around Dissolved Nonpolar Groups. *Proc. Natl. Acad. Sci. U. S. A.* **2009**, *106*, 12230–4.

(16) Rankin, B. M.; Ben-Amotz, D.; van der Post, S. T.; Bakker, H. J. Contacts Between Alcohols in Water Are Random Rather than Hydrophobic. *J. Phys. Chem. Lett.* **2015**, *6*, 688–692.

(17) Kashtanov, S.; Augustson, A.; Rubensson, J.-E.; Nordgren, J.; Ågren, H.; Guo, J.-H.; Luo, Y. Chemical and Electronic Structures of Liquid Methanol from X-ray Eemission Spectroscopy and Density Functional Theory. *Phys. Rev. B* **2005**, *71*, 104205.

(18) Guo, J.-H.; Luo, Y.; Augustsson, A.; Kashtanov, S.; Rubensson, J.-E.; Shuh, D. K.; Ågren, H.; Nordgren, J. Molecular Structure of Alcohol-Water Mixtures. *Phys. Rev. Lett.* **2003**, *91*, 157401.

(19) Nishi, N.; Takahashi, S.; Matsumoto, M.; Tanaka, A.; Muraya, K.; Takamuku, T.; Yamaguchi, T. Hydrogen-Bonded Cluster Formation and Hydrophobic Solute Association in Aqueous Solutions of Ethanol. *J. Phys. Chem.* **1995**, *99*, 462–468.

(20) Bakó, I.; Jedlovszky, P.; Pálinkás, G. Molecular Clusters in Liquid Methanol: a Reverse Monte Carlo Study. *J. Mol. Liq.* **2000**, *87*, 243–254.

(21) Soper, A. Empirical Potential Monte Carlo Simulation of Fluid Structure. *Chem Phys.* **1996**, *202*, 295–306.

(22) Soper, A. K. Partial Structure Factors from Disordered Materials Diffraction Data: An Approach Using Empirical Potential Structure Refinement. *Phys. Rev. B* **2005**, *72*, 104–204.

(23) Soper, A. K. *GudrunN and GudrunX: Programs for Correcting Raw Neutron and X-ray Diffraction Data to Differential Scattering Cross Section*; RAL Rep. RAL-TR-2011-013, STFC Rutherford Appleton Laboratory: Didcot, UK, 2011.

(24) Soper, A. K. Inelasticity Corrections for Time-of-Flight and Fixed Wavelength Neutron Diffraction Experiments. *Mol. Phys.* **2009**, *107*, 1667–1684.

(25) Soper, A. K. The Radial Distribution Functions of Water as Derived from Radiation Total Scattering Experiments: Is There Anything We Can Say for Sure? *ISRN Phys. Chem.* **2013**, *2013*, 1–67.

(26) McGreevy, R. L.; Pusztai, L. Reverse Monte Carlo Simulation: A New Technique for the Determination of Disordered Structures. *Mol. Sim.* **1988**, *1*, 359–367.

(27) Lenton, S.; Walsh, D. L.; Rhys, N. H.; Soper, A. K.; Dougan, L. Structural Evidence for Solvent-Stabilisation by Aspartic Acid as a Mechanism for Halophilic Protein Stability in High Salt Concentrations. *Phys. Chem. Chem. Phys.* **2016**, *18*, 18054–18062.

(28) Rhys, N. H.; Gillams, R. J.; Collins, L. E.; Callear, S. K.; Lawrence, M. J.; McLain, S. E. On the Structure of an Aqueous Propylene Glycol Solution. *J. Chem. Phys.* **2016**, *145*, 224504.

(29) McLain, S. E.; Soper, A. K.; Watts, A. Structural Studies on the Hydration of L-Glutamic Acid in Solution. *J. Phys. Chem. B* **2006**, *110*, 21251–21258.

(30) Rhys, N. H.; Bruni, F.; Imberti, S.; McLain, S. E.; Ricci, M. A. Glucose and Mannose: A Link between Hydration and Sweetness. *J. Phys. Chem B* **2017**, acs.jpcb.7b03919.

(31) Mclain, S. E.; Soper, A. K.; Terry, A. E.; Watts, A. Structure and Hydration of L-Proline in Aqueous Solutions. *J. Phys. Chem. B* **2007**, 4568–4580.

(32) Lenton, S.; Rhys, N. H.; Towey, J. J.; Soper, A. K.; Dougan, L. Highly Compressed Water Structure Observed in a Perchlorate Aqueous Solution. *Nature Comm.* **2017**, *8*.

(33) Haughney, M.; Ferrario, M.; Mcdonaldt, I. R. Molecular-Dynamics Simulation of Liquid Methanol. *J. Phys. Chem.* **1987**, *91*, 4934–4940.

(34) Gao, J.; Habibollazadeh, D.; Shao, L. A Polarizable Intermolecular Potential Function for Simulation of Liquid Alcohols. *J. Phys. Chem.* **1995**, *99*, 16460–16467.

(35) Stewart, J. P. Stewart Computational Chemistry - MOPAC Home Page. `http://openmopac.net/`.

(36) Berendsen, H. J. C.; Grigera, J. R.; Straatsma, T. P. The Missing Term in Effective Pair Potentials. *J. Phys. Chem.* **1987**, *91*, 6269–6271.

(37) Hummer, G.; Soumpasis, D. M.; Neumann, M. Computer Simulation of Aqueous Na-Cl Electrolytes. *J. Phys.: Condens. Matter* **1994**, *6*, A141–A144.

(38) Soper, A. K. Empirical Potential Structure Refinement - EPSRshell: a User's Guide. Version 18 - May 2011. *RAL Technical Report: RAL-TR-2011-012* **2011**, RAL–TR–2011–012.

(39) Soper, A. K. The Excluded Volume Effect in Confined Fluids and Liquid mixtures. *J. Phys.: Condens. Matter* **1997**, *9*, 2399–2410.

(40) Moore, E. B.; Molinero, V. Growing Correlation Length in Supercooled Water. *J. Chem. Phys.* **2009**, *130*, 244505.

(41) Errington, J. R.; Debenedetti, P. G. Relationship between Structural Order and the Anomalies of Liquid Water. *Nature* **2001**, *409*, 318–321.

(42) Svishchev, I. M.; Kusalik, P. G. Structure in Liquid Water: A Study of Spatial Distri-
bution Functions. *J. Chem. Phys.* **1993**, *99*, 3049–3058.

(43) Finney, J. L.; Hallbrucker, A.; Kohl, I.; Soper, A. K.; Bowron, D. T. Structures of High
and Low Density Amorphous Ice by Neutron Diffraction. *Phys. Rev. Lett.* **2002**, *88*,
225503.

(44) Towey, J. J.; Soper, A. K.; Dougan, L. Molecular Insight Into the Hydrogen Bonding
and Micro-Segregation of a Cryoprotectant Molecule. *J. Phys. Chem. B* **2012**, *116*,
13898–13904.

(45) Davis, J. G.; Gierszal, K. P.; Wang, P.; Ben-Amotz, D. Water Structural Transformation
at Molecular Hydrophobic Interfaces. *Nature* **2012**, *491*, 582–585.

(46) Titantah, J. T.; Karttunen, M. Long-Time Correlations and Hydrophobe-Modified
Hydrogen-Bonding Dynamics in Hydrophobic Hydration. *J. Am. Chem. Soc.* **2012**,
134, 9362–9368.

(47) Chandler, D. Interfaces and the Driving Force of Hydrophobic Assembly. *Nature* **2005**,
437, 640–647.

Graphical TOC Entry